Neuron
NeuroResource

Multiplex Cell and Lineage Tracking with Combinatorial Labels

Karine Loulier,[1,2,3] Raphaëlle Barry,[1,2,3] Pierre Mahou,[4,5,6] Yann Le Franc,[1,2,3] Willy Supatto,[4,5,6] Katherine S. Matho,[1,2,3] Siohoi Ieng,[1,2,3] Stéphane Fouquet,[1,2,3] Elisabeth Dupin,[1,2,3] Ryad Benosman,[1,2,3] Alain Chédotal,[1,2,3] Emmanuel Beaurepaire,[4,5,6] Xavier Morin,[7,8,9,*] and Jean Livet[1,2,3,*]
[1]INSERM, U968, Paris 75012, France
[2]Sorbonne Universités, UPMC Univ Paris 06, UMR_S 968, Institut de la Vision, Paris 75012, France
[3]CNRS, UMR 7210, Paris 75012, France
[4]Laboratoire d'Optique et Biosciences, Ecole Polytechnique, Palaiseau 91128, France
[5]CNRS, UMR 7645, Palaiseau 91128, France
[6]INSERM, U696, Palaiseau 91128, France
[7]Ecole Normale Supérieure, Institut de Biologie de l'ENS, IBENS, Paris 75005, France
[8]INSERM, U1024, Paris 75005, France
[9]CNRS, UMR 8197, Paris 75005, France
*Correspondence: xavier.morin@ens.fr (X.M.), jean.livet@inserm.fr (J.L.)
http://dx.doi.org/10.1016/j.neuron.2013.12.016

SUMMARY

We present a method to label and trace the lineage of multiple neural progenitors simultaneously in vertebrate animals via multiaddressable genome-integrative color (MAGIC) markers. We achieve permanent expression of combinatorial labels from new Brainbow transgenes introduced in embryonic neural progenitors with electroporation of transposon vectors. In the mouse forebrain and chicken spinal cord, this approach allows us to track neural progenitor's descent during pre- and postnatal neurogenesis or perinatal gliogenesis in long-term experiments. Color labels delineate cytoarchitecture, resolve spatially intermixed clones, and specify the lineage of astroglial subtypes and adult neural stem cells. Combining colors and subcellular locations provides an expanded marker palette to individualize clones. We show that this approach is also applicable to modulate specific signaling pathways in a mosaic manner while color-coding the status of individual cells regarding induced molecular perturbations. This method opens new avenues for clonal and functional analysis in varied experimental models and contexts.

INTRODUCTION

A major goal in neuroscience is to understand how the complex structure of brain circuits is organized and emerges through development. In this endeavor, visualizing individual neuronal and glial cells within intact nervous tissues and reconstructing their lineage relationships is essential to uncover the developmental constraints exerted on circuit architecture. This requires labels that identify clonally related cells while revealing their morphology. Among available schemes (Buckingham and Meilhac, 2011; Kretzschmar and Watt, 2012), sparse genetic labeling through low titer viral infection (Price et al., 1987) as well as spontaneous or induced sporadic genomic recombination (Magavi et al., 2012; Mathis and Nicolas, 2003; Badea et al., 2003) has become the approach of choice to mark individual progenitor cells and identify their descendants in the nervous system of vertebrate animal models. This strategy has for instance been used in the rodent cortex to demonstrate the lineage relationship between radial glial cells and excitatory neurons (Noctor et al., 2001) and to provide evidence that neurons issued from a common progenitor form preferential synaptic contacts (Li et al., 2012; Ohtsuki et al., 2012; Yu et al., 2009, 2012).

However, with a unique marker, very low labeling density is required to reliably single out individual clones in the central nervous system. At high labeling density, only partial information on clonal limits is accessible (e.g., Kuan et al., 1997; Tan et al., 1995). This prevents one from comparing the lineages and analyzing the interactions of neighboring individual clones. Alternative schemes that use multiple labels to independently mark and track several progenitor cells within a tissue are being increasingly developed. Pioneering studies used DNA barcodes encoded by retroviral libraries for singling out individual neural clones (Walsh and Cepko, 1992, 1993), and methods are emerging to reconstruct lineage based on spontaneous mutations that accumulate in somatic cells (Carlson et al., 2012; Wasserstrom et al., 2008). However, although DNA sequence variants can generate very large numbers of labels, their identification requires tissue disruption. Another approach takes advantage of fluorescent proteins (FPs) of distinct colors to distinguish cells in intact tissue. These FPs can be expressed in a mosaic manner via chimeric animals (e.g., Ueno and Weissman, 2010), mixtures of retroviral particles or transposon vectors (Malide et al., 2012; Weber et al., 2011; Garcia-Marques and Lopez-Mascaraque, 2013), as well as reporter transgenes activated by site-specific recombination systems such as Cre/*lox* (Birling et al., 2009). This latter approach offers versatile possibilities to express FPs within intact and live tissues (Jefferis and

Livet, 2012). The simplest multicolor reporters switch expression from one color to another upon action of Cre recombinase (De Gasperi et al., 2008; Muzumdar et al., 2007). The MADM system uses Cre-mediated interchromosomal recombination to label sibling neural progenitors and their descent with two distinct colors (Tasic et al., 2012; Zong et al., 2005). More than two markers are desirable, however, to secure clonal identification without resorting to extreme sparseness. Brainbow transgenic strategies maximize color output from a single transgene with divergent Cre/*lox* recombination pathways that create a random expression choice among 3–4 spectrally distinct FPs (Livet et al., 2007). One copy of a Brainbow transgene expresses a single FP variant (Rinkevich et al., 2011; Snippert et al., 2010), whereas co-expression of multiple copies yields FP combinations, creating varied colors that distinguish cells (Cai et al., 2013; Kobiler et al., 2010; Livet et al., 2007). In this scheme, recombination of one or more genome-integrated transgenes permanently attributes a random combination of colors to a cell and its progeny. Recent studies performed in nonneural tissues (Ghigo et al., 2013; Rinkevich et al., 2011; Schepers et al., 2012; Snippert et al., 2010; Tabansky et al., 2013) as well as in nonmammalian models (Gupta and Poss, 2012; Hadjieconomou et al., 2011; Hampel et al., 2011; Pan et al., 2013) have demonstrated the usefulness of this approach for tracing cell lineages and assessing progenitor equivalence. Yet its portability for multiplex identification of intermixed clones in the complex environment of the vertebrate brain is hampered in current Brainbow transgenic animals: some lines harbor only a single transgene copy and express a limited palette of 3–4 markers (Ghigo et al., 2013; Rinkevich et al., 2011; Schepers et al., 2012; Snippert et al., 2010); other lines label only certain differentiated cell types (Cai et al., 2013; Livet et al., 2007) or express by default one of three FP labels and are therefore not optimal for sparse labeling (Gupta and Poss, 2012; Pan et al., 2013; Tabansky et al., 2013).

Here we propose methods and reagents to simultaneously label multiple cells or clones with an enhanced palette of combinatorial markers suitable for lineage tracing and live imaging in a broad range of contexts. This toolkit, dubbed multiaddressable genome-integrative color (MAGIC) markers, uses new transposon-based Brainbow transgenes to direct long-term expression of an expanded range of clonal markers that combine both FP colors and subcellular locations. Our approach, directly applicable in a variety of non-genetically tractable models, also provides a way to perturb specific signaling pathways in color-coded genetic mosaics.

RESULTS

New Brainbow Cassettes for Sparse Cre-Dependent Expression of Compartmented Trichromatic Fluorescent Markers

The MAGIC Marker strategy aims to fulfill several partially conflicting criteria: (1) maximized number of labels available to contrast individual cells or clones; (2) expression of well distinct FP markers for optimal signal collection and separation; (3) equilibrated, near-random distribution of these markers in recombined cells; (4) controllable timing and sparseness of the labeling; and (5) label stability during cell division. We designed four constructs expressing cytoplasmic, nuclear, membrane, or mitochondria-targeted FPs under the control of the broadly active *CAG* synthetic promoter (Niwa et al., 1991), referred to below as *Cytbow, Nucbow, Palmbow*, and *Mitbow* (Figure 1). These transgenes offer three mutually exclusive recombination possibilities that each switch on a distinct FP (Figure 1A): the orange-red tdTomato or mCherry (Shaner et al., 2004), the yellow-green mEYFP (Zacharias et al., 2002), and the blue-green mCerulean (Rizzo et al., 2004) or mTurquoise2 (Goedhart et al., 2012). A nuclear version of the UV-shifted EBFP2 (Ai et al., 2007) is expressed in the unrecombined state. This design allows for labeling recombined cells—and only these cells—with three randomly expressed FP markers (conveniently coded as red, green, and blue) while leaving the far-red channel available for orthogonal labels.

We first tested the new Brainbow constructs in vitro (Figure S1 available online). In HEK293 cell lines, expression switched from EBFP2 to the three other FPs upon transfection with Cre (Figure S1A). Depending on the line, FP expression was either mutually exclusive or combinatorial, as expected from single or multicopy transgene integration. Importantly, color labels were maintained during clonal expansion, validating their usage as lineage reporters (Figure S1B). In parallel, we generated transgenic mouse lines with the *CAG*-driven *Cytbow* and *Nucbow* transgenes. We induced recombination by crossing these animals with mice expressing the inducible CreER recombinase and administrating low doses of tamoxifen ligand during gestation or at birth. FP expression was analyzed in the postnatal cortex several days after tamoxifen injection (Figures S1C and S1D). Recombined cells expressing each of the three recombination outcomes in a mostly mutually exclusive manner were highlighted over an unstained background. Remarkably, sparse clusters of cells expressed the same marker, consistent with activation of the transgene in single progenitors followed by stable inheritance of FP labels during clonal expansion.

Multicolor Labeling of Neural Cells with Embryonic Electroporation

For wider applicability of the new transgenes and expression of larger numbers of FP combinations in the nervous system, we sought to introduce the new vectors in embryonic neural progenitors by electroporation. To render the labels heritable for lineage-tracking purposes, we created genome-integrative versions of the four transgenes in which the whole cassette is framed by minimal 5′ and 3′ transposition sequences of the *Tol2* (T2) or *PiggyBac* (PB) transposons (Figures 1A and 1B; Lacoste et al., 2009; Sato et al., 2007; Yoshida et al., 2010). The transgenes were electroporated in the embryonic mouse forebrain or chicken spinal cord together with a tamoxifen-inducible Cre (Matsuda and Cepko, 2007) or self-excising Cre (*se-Cre*, modified from Mähönen et al., 2004), chosen to minimize the duration of recombination, in the presence or absence of a transposase expression vector (Figures 1C–1E). Within the electroporated area (highlighted by the default-expressed nuclear EBFP2), Cre recombination triggered expression of cyan, yellow, or red FP, yielding a semisparse mosaic of color combinations (Figure 1C). Each transgene addressed FPs in the expected subcellular locations: *Cytbow* expression revealed cell morphology, *Palmbow*

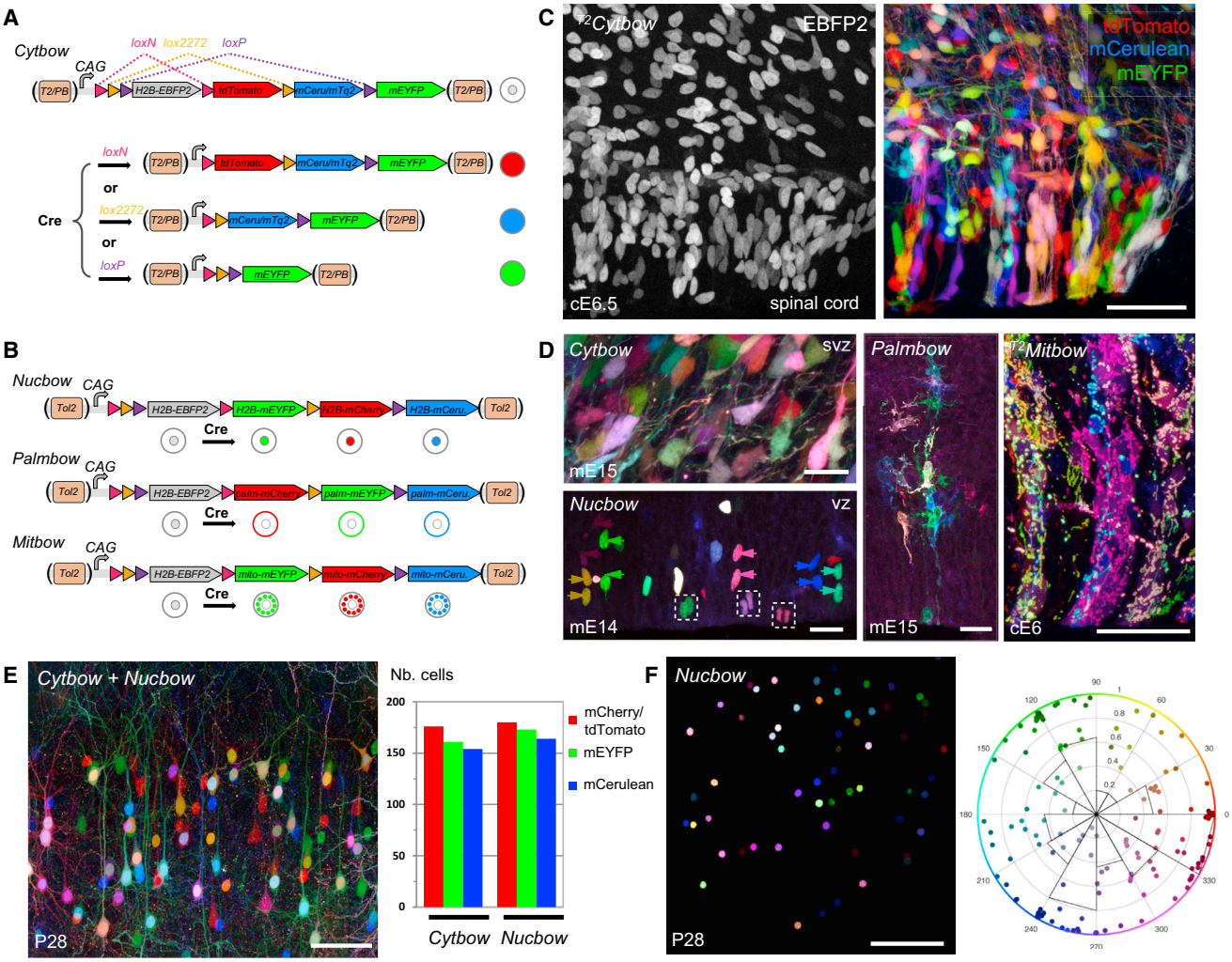

Figure 1. Transposable Brainbow Vectors for Compartmented Cre-Dependent Multicolor Labeling

(A) Brainbow transgenes for balanced trichromatic labeling. All transgenes express by default a nuclear EBFP2 under the control of a *CAG* promoter. Three recombination possibilities created by alternated pairs of incompatible *lox* sites each trigger expression of a distinct FP: mCerulean/mTurquoise2 (mCeru/mTq2), mEYFP, or tdTomato/mCherry. 5′ and 3′ *Tol2* (T2) or *PiggyBac* (PB) transposition sequences frame the transgenes.

(B) Brainbow transgene variants expressing FPs with specific subcellular addresses: cytoplasm (*Cytbow*), nucleus (*Nucbow*), membrane (*Palmbow*), and mitochondria (*Mitbow*). See Figure S1 for validation of the transgenes in cell and mouse lines.

(C) Transverse section of an E6.5 chick spinal cord electroporated at E2 with ^{T2}*Cytbow* along with *se-Cre* and *Tol2*, showing the default-EBFP2 (left) and the recombination outcomes mCerulean, mEYFP, and tdTomato (right).

(D) Embryonic electroporation of the *CAG-Brainbow* transgenes in the mouse cortex and chick spinal cord yields semisparse multicolor labeling in the ventricular (VZ) and subventricular zone (SVZ). *Cytbow* and *Palmbow* were electroporated with *Cre* in E13 and E14 mouse cortices, respectively, and imaged at E15. *Nucbow* was electroporated at E13 in *CAG-CreERTM* mice 24 hr after tamoxifen administration and imaged at E14. Pairs of sister cells (arrows) as well as cells still in mitosis (framed) express similar colors. ^{T2}*Mitbow* was electroporated in E2 chick spinal cords and analyzed at E6.

(E) Cortical pyramidal neurons of a P28 *CAG-CreERTM* mouse electroporated with both *Cytbow* and *Nucbow* at E15, 24 hr after tamoxifen induction, imaged by two-photon microscopy. Histogram quantifies cells expressing cytoplasmic or nuclear tdTomato/mCherry, mEYFP, and mCerulean among all 385 labeled pyramidal neurons found in the data set. See Figure S2 for color-based segmentation of labeled cells.

(F) Micrograph of a P28 mouse brain coelectroporated with *Nucbow* and *Cre* plasmids at E14. Polar plot shows the mean Hue/Saturation values of 150 labeled cells in the data set. Histogram represents the normalized proportion of cells in 30° sections of hue values.

Scale bars represent 50 μm (C), 40 μm (D), or 100 μm (E and F).

labels highlighted membranes and processes, *Nucbow* markers were restricted to nuclei or condensed chromosomes during mitosis, and mitochondria of individual cells were homogenously stained with *Mitbow* (Figure 1D).

In the absence of transposase, episomal transgenes could be used shortly (24 hr) after electroporation to identify nearby sister cells in the ventricular zone (VZ) of the cortical neuroepithelium, in the course of or shortly after division (see *Nucbow* in

Figure 1D). Although these episomal plasmids quickly diluted in cycling progenitors, labels were maintained until adult stages in neural cells born at the time of electroporation, as indicated by their position in cortical layer II–III (Figures 1E and 1F). This allowed us to assay the balance between the three recombination outcomes. A survey of 385 labeled pyramidal cells in an adult cortex data set showed equilibrated expression of the three FPs expressed by the *Cytbow* and *Nucbow* transgenes, indicating that the recombination choice within each Brainbow transgene was largely random (Figure 1E). Coexpression of FPs in varied proportions resulted in widely distributed hues, as demonstrated by quantitative color analysis of 150 *Nucbow*-labeled pyramidal neurons (Figure 1F).

The additional information provided by color labels expressed from the *Cytbow* transgene could be used both for manual and semiautomated image segmentation (Figure S2). In mouse embryos, multicolor labels made it possible to distinguish and manually trace multipolar cells and their fine processes in densely labeled areas of the embryonic cortical subventricular zone (SVZ) (Figure S2A). In adult animals, color contrasts could be used by semiautomated algorithms to resolve pyramidal cells and their neurites (Figure S2B).

Transposase-Mediated Genomic Integration of Brainbow Transgenes in Neural Progenitors

Lineage tracking over multiple rounds of cell division is most conveniently obtained with indelible genome-encoded labels that replicate during cell division. To achieve their chromosomal integration, we electroporated the transposon-based Brainbow vectors along with plasmids encoding the corresponding transposase (Tol2 or PB) and the Cre recombinase in chick and mouse embryos.

In E4 chick spinal cord sections, 48 hr after electroporation with ^{T2}*Cytbow*, *Tol2* transposase, and *se-Cre*, color labels were maintained in the VZ, site of embryonic neurogenesis (Figure 2). Time-lapse imaging showed that the color of dividing cells was inherited by their two daughters (n = 5, Figure 2 and Movie S1). Radially oriented groups of 2–4 juxtaposed bipolar cells, consistent with their sharing a clonal origin, were also labeled with similar colors (Figures 2 and S3A). Thus, the proportions of FP markers expressed by neural progenitors electroporated with integrative Brainbow vectors were not grossly altered by cell division.

To assess the long-term stability of MAGIC markers, we analyzed later time points after electroporation of ^{T2}*Cytbow* or ^{T2}*Nucbow* (Figure 3). In E6–E10 chick spinal cords, i.e., 4–8 days after electroporation, intensely and uniformly labeled radial streams of cells running from the VZ to the outer layers of the neural tube were apparent in whole-mount preparations (n = 6, Figures 3A, 3C, and 3D) and in transverse sections (Figures 3B and S3B). In the most sparsely labeled samples, radial streams exhibiting a homogenous color were often completely isolated spatially from other labeled cells (Figures 3A, 3C, and S3B), consistent with clonal patterns observed by retroviral methods (Leber and Sanes, 1995). In densely labeled samples, despite extensive intermixing, color contrasts among neighboring streams provided a readout of their frontiers on a cell-by-cell basis (Figure 3D). In contrast, no radial streams were visible in absence of transposase and only residual expression was observed in the VZ, whereas strong labeling appeared restricted to early-born postmitotic neuronal cells carrying episomal transgene copies (n = 3, Figures 3A and 3B). This demonstrates that transposase-mediated genomic integration of Brainbow transgenes allows both stable maintenance of color labels in neural progenitors over multiple rounds of cell division and transmission of these same labels in the progenitors' descent.

We also tested the Brainbow transposons in the mouse cerebral cortex (Figures 3E–3G and S3). Without transposase, 4 to 5 days after electroporation at E13 with the ^{T2}*Cytbow* transgene and *se-Cre* recombinase, episomal plasmids labeled only neurons born shortly after electroporation whereas expression in ventricular progenitors had largely disappeared (Figure 3E). In contrast, in the presence of the corresponding transposase, genomic integration of ^{T2}*Cytbow* or ^{PB}*Cytbow* was apparent from expression in cells located at the ventricular surface or migrating radially toward external layers (Figures 3F, 3G, and S3D, n = 3 for each condition).

Hence, in situ genomic integration of electroporated Brainbow vectors with both the Tol2 and PB transposition systems marks cycling neural progenitors with a large panel of distinct colors that are maintained through cell division over extended periods of development.

Long-Term Tracking of Embryonic Progenitors Giving Rise to Glial and Postnatal Neural Lineages with MAGIC Markers

To determine whether color labels introduced during embryonic neurogenesis could be used to follow cell lineage until further time points in development, we analyzed postnatal mice in which the dorsal VZ had been electroporated at E13 with ^{T2}*Cytbow* (Figure 4). Around birth, progenitors of the dorsal telencephalon become mostly gliogenic except for the few that participate in postnatal neurogenesis, such as those generating a fraction of olfactory bulb interneurons (Kohwi et al., 2007). At stages P7–P28, in addition to neurons, many glial cells were labeled in the cortex of electroporated animals, including astrocytes and oligodendrocytes, demonstrating that their parent stem cells had been targeted (n = 6 mice, Figures 4A, 4B, and S4). These cell types were not observed with nonintegrative vectors. In sparsely labeled P7–P28 samples, isolated clusters of 2–14 astrocytes expressing an identical color were apparent (4.4 ± 2.3 cells at P22, n = 63), similar to those observed by other approaches (Garcia-Marques and Lopez-Mascaraque, 2013). These astrocytes were labeled with 6–10 colors, consistent with FP coexpression from 2–3 ^{T2}*Cytbow* copies and indicating that they originated from multiple distinct progenitors (Figure S4A). We analyzed a densely labeled 800 × 1,000 × 350 μm^3 volume imaged with two-photon microscopy that covered the entire depth of the cerebral cortex of a 4-week-old mouse (Mahou et al., 2012). Segmentation and color analysis of 457 astrocytes within this data set showed that same-color astrocytes formed clusters with a preferred columnar orientation (Figures 4B and S4D), suggesting that clonally related astrocytes undergo localized radial expansion during the phase of cortical astroglia proliferation (Ge et al., 2012) and/or coordinated migration during development.

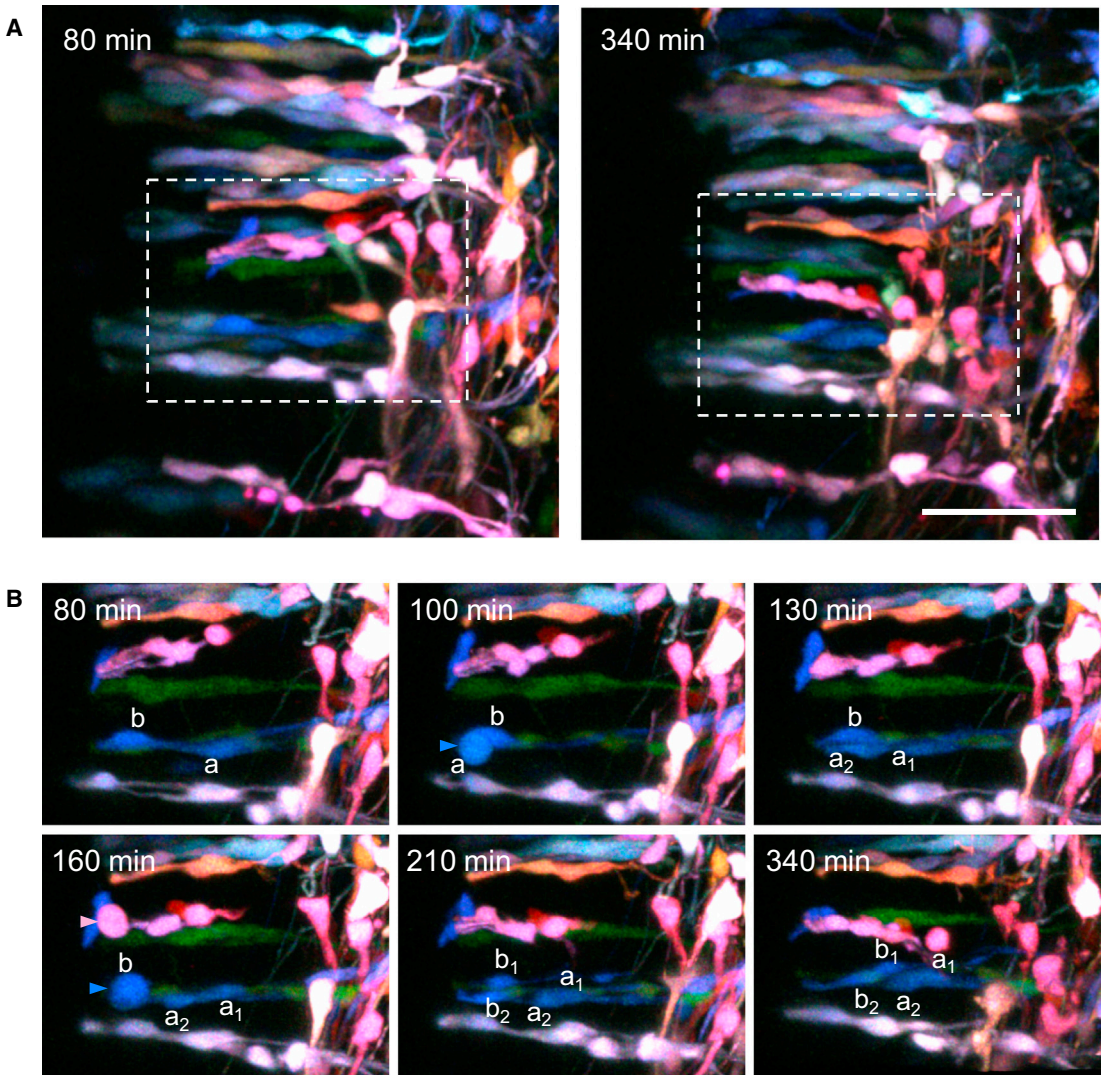

Figure 2. Time-Lapse Two-Photon Imaging of Dividing Neural Progenitors in the Embryonic Chick Spinal Cord

E4 chick embryo transverse neural tube section imaged by two-photon microscopy 48 hr after electroporation with ^{T2}*Cytbow, se-Cre*, and *Tol2* transgenes.

(A) General view of the section at two time points (projection of a 200 μm thick volume). Streams of bipolar neural progenitors contacting the ventricular surface (left) are observed that share a same color. Scale bar represents 50 μm.

(B) Time-lapse series of the area boxed in (A) (projection of a 60 μm thick subvolume). Two progenitors (*a* and *b*) in a blue clone divide at 100 min and 160 min (blue arrowheads), producing four cells (*a1* and *a2*, *b1* and *b2*) that maintain the same color. Another cell divides at 160 min within a pink clone (pink arrowhead). See full time-lapse as Movie S1.

In young and mature mice, color labels also persisted in the SVZ site of postnatal neurogenesis and source of the interneurons that migrate along the rostral migratory stream (RMS) to populate the olfactory bulb (OB) (Figure 4C). Cells in the SVZ, RMS, and granule neurons in the OB were marked with a similar palette of multicolor labels, consistent with their known lineage relationship (n = 5 mice, Figure 4C). However, in contrast with astrocytes, no clustering of same-color cells was apparent in the RMS and OB, suggesting that lineage did not constrain the cells' spatial arrangement in these two areas. At the SVZ level, intermingled cells of different colors were found locally in similar numbers, indicating absence of clonal "takeover" in the precursors of the perinatal forebrain SVZ. Interestingly, in the light of previous studies showing that electroporation targets cells in S/M phase (Stancik et al., 2010), the labeling of postnatal SVZ cells and OB neurons after electroporation of the cortical VZ at E13 suggests that their ancestor was mitotically active at that stage.

Functional Analysis with MAGIC Markers

Brainbow transgenes create a Cre-dependent stochastic choice among several genes, made at the individual cell level. This situation is ideal for genetically manipulating specific molecular determinants in a mosaic manner. In this type of analysis, MAGIC

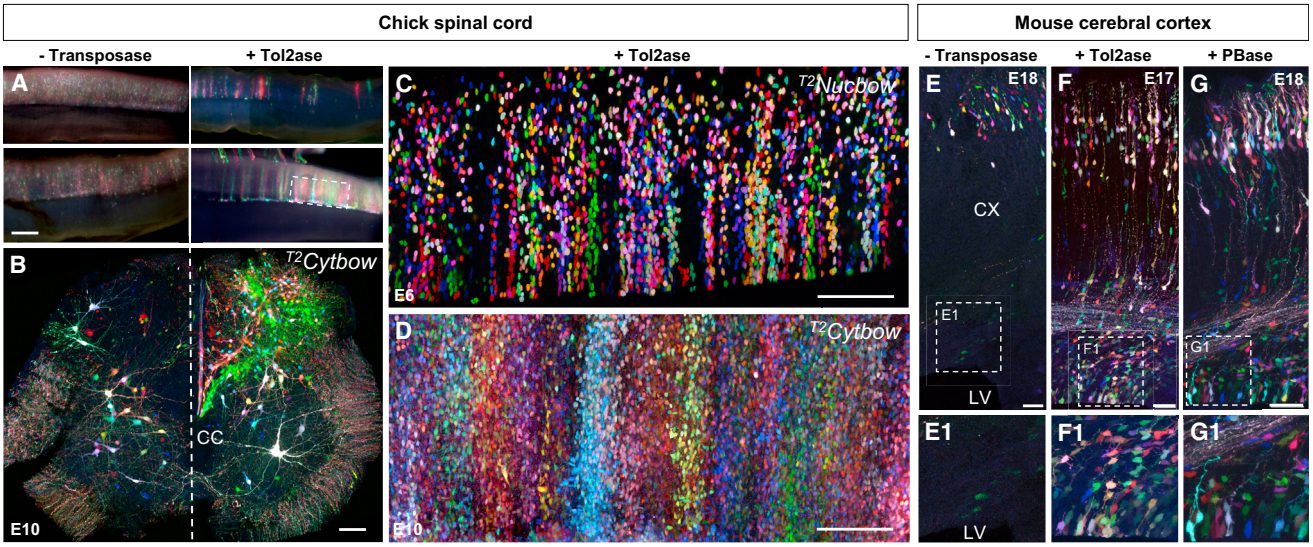

Figure 3. Transposase-Mediated Genome Integration of Brainbow Transgenes

(A) Whole E10 chick spinal cords (dorsal views) electroporated at E2 with *T2Cytbow* and *se-Cre* plasmids in absence of transposase show stochastic multicolor labeling (left). Coelectroporation with *Tol2* transposase (Tol2ase) labels clonal streams of cells migrating from the midline (right).

(B) Transverse section of an E10 spinal cord electroporated at E2 with *T2Cytbow* and *se-Cre* on the left side, and *T2Cytbow, se-Cre*, and *Tol2* transposase on the right side. Episomal *T2Cytbow* labels only early-born differentiated neurons (left). Genome integration is apparent on the side electroporated with transposase from colored streams of cells originating from the ventricular zone (right). Projection of a 100 μm confocal stack. CC, central canal.

(C and D) Whole embryonic chick spinal cords electroporated with *T2Nucbow* (E6 in C) and *T2Cytbow* (E10 in D) along with *Tol2* and *Cre* recombinases at E2 (dorsal view). Clonal streams of cells originating from the midline are visible in confocal (top) and two-photon images (640 × 290 × 450 μm^3 volume, bottom).

(E–G) Comparison of *T2Cytbow* and *PBCytbow* expression with and without transposase in the embryonic mouse cortex. Five days after electroporation of cortical progenitors at E13 with episomal *T2Cytbow* and *se-Cre*, dividing progenitors in the ventricular zone (VZ) bordering the lateral ventricle (LV) have almost completely lost their labels (E and E1). Coelectroporation of *T2Cytbow* and *Tol2* (F and F1) or *PBCytbow* and *PB* (G and G1) transposase allows for maintaining color labels in cells of the dorsal VZ and their radially migrating descendants.

See Figure S3 for other examples. Scale bars represent 500 μm (A) or 100 μm (B–G).

markers make it possible to compare control and experimental conditions within a same sample, using colors to read the status of each cell regarding the induced perturbation. To evaluate the potential of this strategy, we devised an experiment to interfere with mitotic spindle positioning in neural progenitors via expression of a dominant-negative form of the G protein signaling modulator LGN (GPSM2). We designed a *Tol2*-transposable Brainbow construct in which this dominant-negative (dnLGN) was expressed as one of the recombination outcomes, along with the fluorescent protein mCerulean (Figure 5). At E17, 3 days after electroporation of this *T2LGNbow* or a control *T2Cytbow* plasmid along with *se-Cre* and *Tol2*, cells expressing all three recombination outcomes were apparent in the cortical wall (Figure 5A). However, in animals electroporated with *T2LGNbow*, cells in the VZ mostly expressed mEYFP and/or tdTomato whereas cells expressing dnLGN, marked with mCerulean, were rare or absent (Figure 5A). Cell counts further confirmed that mCerulean-labeled cells were markedly decreased in the VZ compared to the *T2Cytbow* construct ($n \geq 2$ animals, $p = 0.0043$, two-tailed p value, Mann-Whitney test), while other colors were not significantly affected (Figure 5B). A reciprocal increase of mCerulean-labeled cells was apparent in the upper cortical plate. This is consistent with results obtained in *LGN* knockout mice (Konno et al., 2008) and with the notion that inducing a switch from the predominantly planar to more oblique spindle orientation favors the production of outer radial glia (oRG) over apical radial glia (RG) (Figure 5C; Shitamukai et al., 2011). Thus in addition to anatomical and cell-lineage purposes, integrative Brainbow transgenes can be used for creating and analyzing mosaic perturbations of specific molecular pathways.

Color-Based Resolution of Spatially Intermixed Clones

The power of MAGIC markers to identify and distinguish clones of cells critically depends on their stability and discriminability.

To provide a quantitative assessment of cell-to-cell variation in FP expression within individual Brainbow-labeled clones, we analyzed E10 chick spinal cords labeled in a semisparse manner at E2 with *T2Cytbow* (Figure 6). In transverse sections, radial streams of labeled cells originating from restricted areas of the VZ were visible (Figure 6A). Groups of cells harboring similar colors were apparent, typically containing one or a few juxtaposed ventricular progenitors and many postmitotic cells, as expected in expanding clones. In the sample shown in Figure 6A, we quantified the relative proportions of red, blue, and green FP expression in 342 segmented cells (Figure 6B). This revealed five distinct clones of 18–133 cells displaying clustered FP proportions, as confirmed by automated *k*-means clustering analysis (intracluster dispersion < 4%, intercluster distance ≥ 20%). These same groups of cells were also identifiable by their

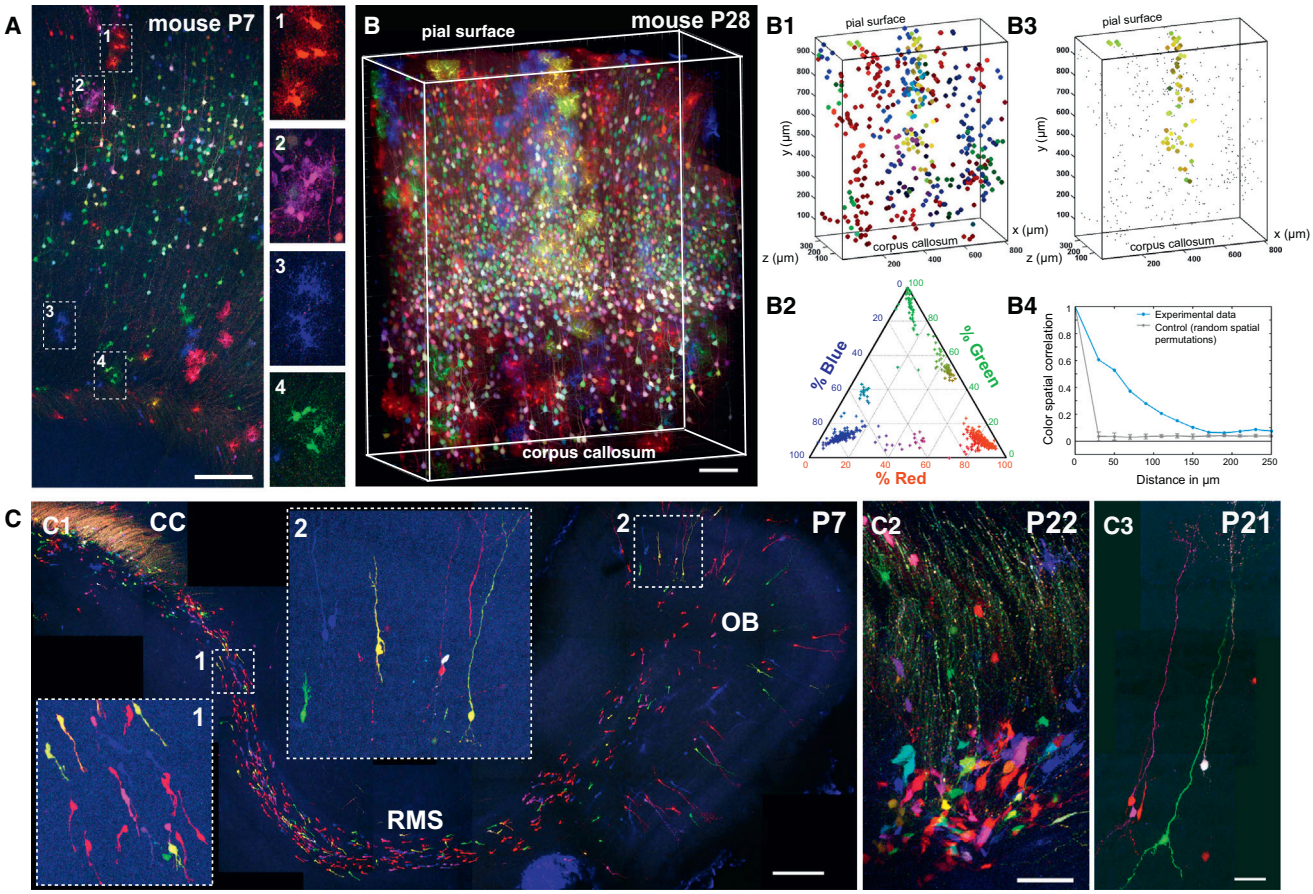

Figure 4. Color-Based Multiplex Lineage Tracking with Integrative Brainbow Transgene

(A and B) In utero electroporation of ^{T2}*Cytbow* in E13 mice labels cortical neurons and astrocytes with multiple colors at P7 (A) and P28 (B).

(A) At P7, astrocytes expressing the same color typically form small clusters of 2–5 cells (see examples 1–4).

(B) Color analysis of astrocytes in a 800 × 1,000 × 350 μm^3 P28 two-photon data set. 457 labeled astrocytes found in the volume (B1) express 6 distinct FP mixtures (red, green, blue, and intermediate colors) (B2). Cells of a same color display a radial columnar organization (B3). Pairwise correlation of the cells' spatial and color distances confirms that astrocytes of nearby colors form clusters, with a characteristic correlation length of 150 μm (error bars: SD of ten random spatial permutations) (B4).

(C) Electroporation of ^{T2}*Cytbow* at E13 in the mouse cortical VZ yields labeling of neuroblasts migrating along the rostral migratory stream (RMS) toward the olfactory bulb (OB) (P7 in C1), their progenitors in the roof of the SVZ (P22 in C2), and fully differentiated OB interneurons (P22 in C3). Interneurons migrating along the RMS or integrated in the OB do not cluster with same color cells.

See Figure S4 for complement. Scale bars represent 200 μm (A, B, C1) or 50 μm (C2, C3).

clustered distribution in RGB tridimensional space, or equivalently, their close hue and saturation values (Figure S5, Movie S2). Each of the five clones identified by this color analysis could then be plotted and analyzed separately (Figures 6C and 6D), showing that they had dispersed in a similar manner and shared common territories within the spinal cord. Hence, even in the case of FP combinations expressed from multiple transgene copies, the recombination signature borne by Brainbow-labeled cells that share a same ancestry results in clustered trichromatic outputs. These specific spectral signatures subdivide the labeling pattern in a lineage-related manner, making it possible to single out clones that originate from juxtaposed neural progenitors even in the case of extensive spatial intermixing.

To explore the relative frequencies of combinatorial FP labels, we imaged whole-mount E6 spinal cords sparsely labeled with ^{T2}*Nucbow* in which large numbers of neural clones could be unambiguously singled-out from a same data set. We focused on the example shown in Figure 6E, in which we identified 61 clones based on their spatial position and color. We plotted the mean RGB values of 676 cells from these clones as a function of their position along the antero-posterior axis (Figure 6F). The cells expressed a large range of FP values that clustered for individual clones (Figures 6F and S5). The clones showed limited dispersion in FP relative proportions, occupying in average 1.1% ± 1.4% of the RGB ternary plot surface; this indicated a theoretical maximum of ~90 discriminable clones, assuming a safe minimal distance between clones of 6 standard deviations in each color channel (see Supplemental Experimental Procedures). A density map of the clones' centroid position in the RGB ternary

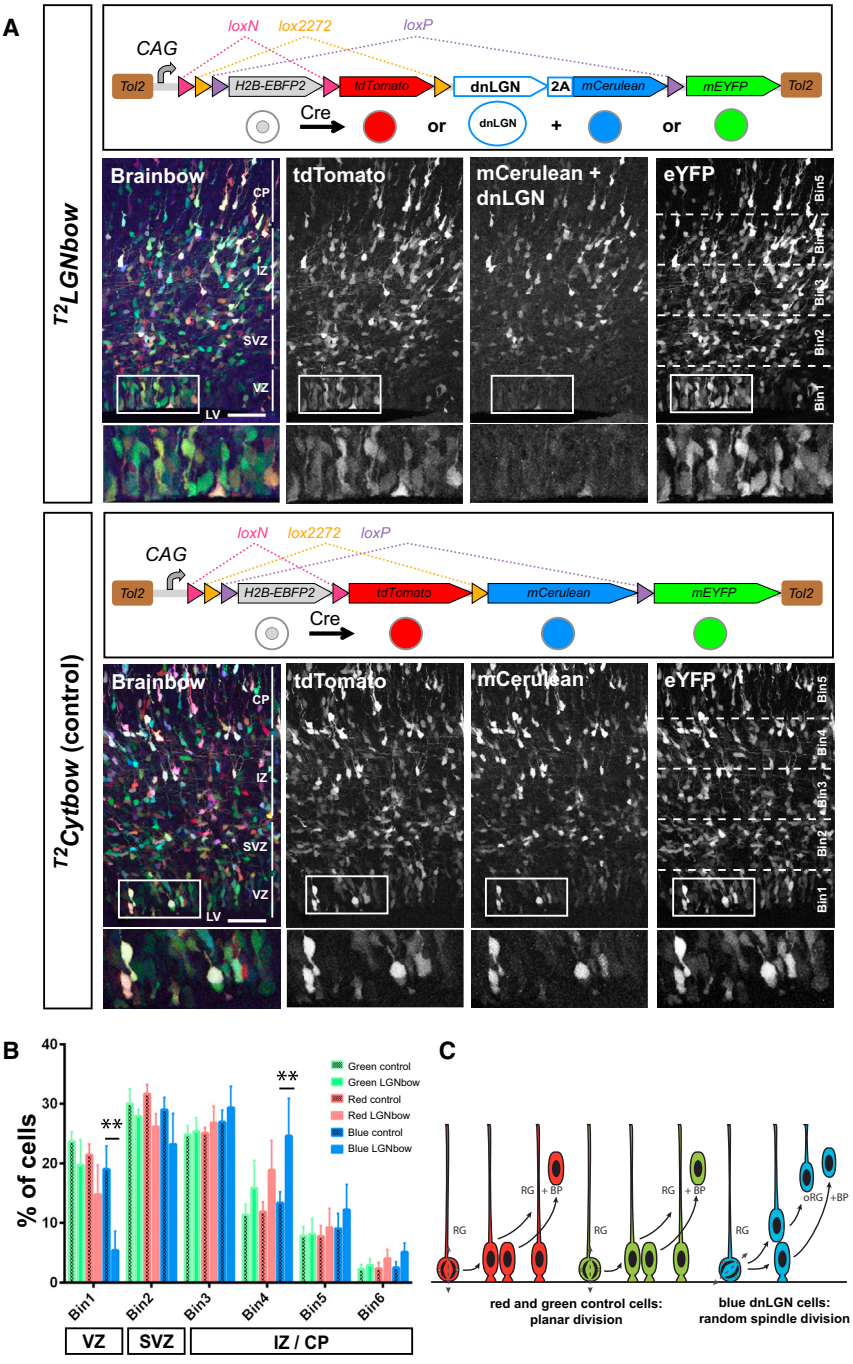

Figure 5. Color-Coded Mosaic Perturbation of LGN Function with Brainbow

(A) The *T2LGNbow* transgene (top), derived from *T2Cytbow* (bottom), bears a modified blue cassette that expresses a dominant-negative form of LGN (dnLGN) along with mCerulean, using a 2A peptide cleavage sequence. Electroporation of *T2LGNbow* in E14 mouse cortical progenitors yields a decrease of mCerulean$^+$ cells located in the VZ at E17 (bin 1, framed insets) compared to control littermates electroporated with *T2Cytbow*. The distribution of tdTomato$^+$ and mEYFP$^+$ cells in *T2LGNbow*- and *T2Cytbow*-electroporated brains shows no apparent difference.

(B) Distribution of tdTomato$^+$, mEYFP$^+$, and mCerulean$^+$ cells along the cortical wall (divided into six equivalent bins from the ventricle to the pial surface; bars represent mean ± SD). A significant decrease is observed in the percentage of blue cells in the VZ of *T2LGNbow*-electroporated cortices (bin 1) compared to control littermates ($n \geq 2$, $^{**}p = 0.0043$, two-tailed p value, Mann-Whitney test) whereas no difference can be seen among mEYFP$^+$ and tdTomato$^+$ cells. Concomitantly, a significant increase in blue cells is observed in bin 4.

(C) Model for the depletion of blue cells from the apical surface. Red and green cells: asymmetrically dividing radial glial cells (RG) predominantly divide in a planar fashion in the E14 mouse cortex, leading to equal partitioning of apical attachments. The daughter cell that retains the basal attachment remains an apical RG, while its sister delaminates to become a basal progenitor (BP). Blue cells: upon dnLGN expression, spindle orientation is randomized; the basal-most daughter retains a basal attachment but loses the apical junctions and quickly migrates basally to adopt an outer radial glial (oRG) identity; the apical-most daughter later delaminates and migrates basally as a BP.

Abbreviations: CP, cortical plate; IZ, intermediate zone; SVZ, subventricular zone; VZ, ventricular zone. Scale bars represent 100 μm.

plot surface confirmed that FP combinations were not equiprobable (Figure 6G). The most frequent labels in this data set corresponded to expression of a single FP (56% of the clones), suggesting frequent occurrence of single-copy transgene integration. In addition, many combinations resulting from coexpression of ≥2 FPs formed specific labels that rarely overlapped with other clones. For instance, in a pairwise comparison of all clones in the data set, we found that 11/61 (18%) expressed combinations that overlapped with as few as 0–1 clones.

Hence, trichromatic labeling improves clonal resolution over classical labeling approaches based on a single marker, making it possible to single out multiple neighboring clones within a same sample. Here, the enhancement in discriminative power ranged from 4-fold (18/61 = 29% clones only expressing CFP) to >60-fold (for unique FP combinations), specific marker combinations having stronger discriminatory power than others. As shown in the above examples, we expect that complex colors resulting from coexpression of ≥2 transgenes should provide the most reliable output for clonal analysis with Brainbow transposons. The discriminatory power of trichromatic labels should in addition depend on the density of labeling and the spatial intermixing between clones (see Discussion).

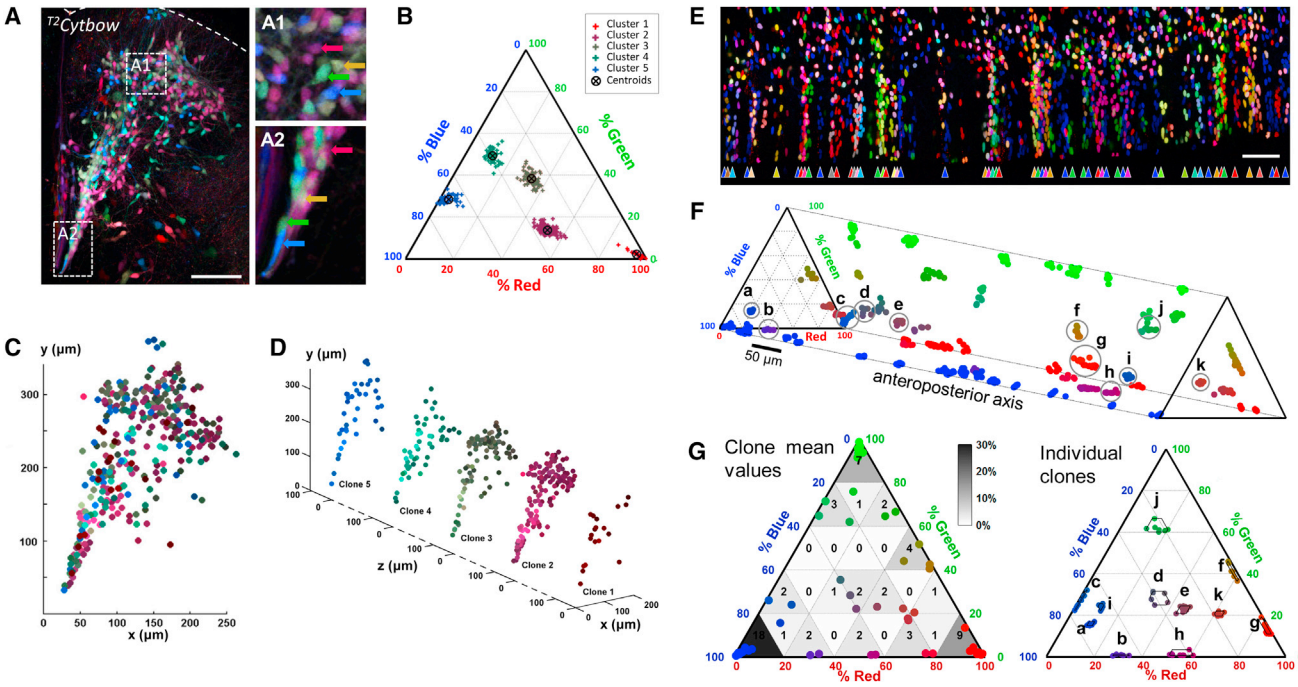

Figure 6. Color-Based Resolution of Spatially Intermixed Clones

(A) Dorsal quadrant of an E10 chick spinal cord electroporated at E2 with the *T2Cytbow* transposon. Labeled cells with hues similar to those migrating radially away from the midline (A1) are found attached to the ventricular surface (A2).

(B) Analysis of normalized RGB values (relative contribution of each FP to the global signal) for 342 labeled cells originating from the same ventricular subarea. *k*-means clustering analysis with automated selection of *k* confirmed identification of five clusters (SD < 4%) expressing distant (≥20%) color labels (each cluster is represented according to its mean color). Also see Figure S5.

(C) Representation of the 342 analyzed cells according to their mean color and xy position.

(D) Spatial distribution of the five overlapping clonal clusters.

(E) Whole E6 chick spinal cord with semisparse *T2Nucbow* labeling (dorsal view, maximal projection of a 90 μm thick volume). 61 clones of ≥6 cells were identified on the basis of their shared color and radial organization (colored arrowheads).

(F) Plot showing the normalized RGB values of the 61 clones identified in (E) as a function of their position along the x (anteroposterior) axis.

(G) Left: Mean values of the 61 clones. The number of clones found in each 25 subdivisions of the normalized RGB space is indicated, as well as their density (grayscale coding). Right: Examples of 11 clones from (**F**) expressing complex FP combinations (*a*–*k*). Polygons show minimal and maximal values of the clones in each channel.

Scale bars represent 100 μm (A) or 50 μm (E, F).

Expanding Brainbow Markers by Combining FP Color and Subcellular Location

Maximizing clonal resolution with Brainbow transgenes requires the largest possible number of markers. Although FPs with intermediate spectral characteristics can provide an augmented palette of markers (Garcia-Marques and Lopez-Mascaraque, 2013; Malide et al., 2012), spectral overlap compromises their discrimination. Another option is to rely on spatial as well as spectral resolution, by combining FP color and subcellular location (Figure 7). This strategy considerably augments labeling possibilities. For instance, whereas expression of two copies of a single type of trichromatic Brainbow transgene generates only six colors, nine distinct marker combinations are obtained if the two transgenes express FPs targeted to distinct locations. Coexpression of additional copies yields an even greater number of combinations (Figure 7A). Figure 7B shows P22 cortical neurons electroporated with *T2Cytbow* and *T2Nucbow* at E13 that display marker combinations in accordance with expression from ≥2 copies of each vector. To demonstrate the suitability of this approach for clonal tracking, we coelectroporated different types of integrative Brainbow transgenes in the chicken spinal cord at E2 (Figures 7C and 7D). In E10 chick spinal cords transfected with *T2Cytbow* and *T2Nucbow*, clones were identifiable on the basis of specific combinations of cytoplasmic and nuclear colors. Remarkably, dual compartment labeling enabled further discrimination between topologically close clones that would not have been identified as distinct with a single type of label (Figure 7C). Coelectroporation of *T2Mitbow* along with the two other transgenes provided a third type of label, easily distinguishable from cytoplasmic and nuclear stains, which further secured clonal identification (Figure 7D). We evaluated the potential of multiaddressed FPs for tracking clonal dispersion in long-term experiments in E17 chick spinal cords coelectroporated at E2 with *T2Cytbow* and *T2Nucbow*. Within one single transverse section, among many combinations of markers (≥36), several were shared by groups of 13–28 cells confined within circumscribed portions of the neural tube, confirming their belonging to a same clone (Figures 7E

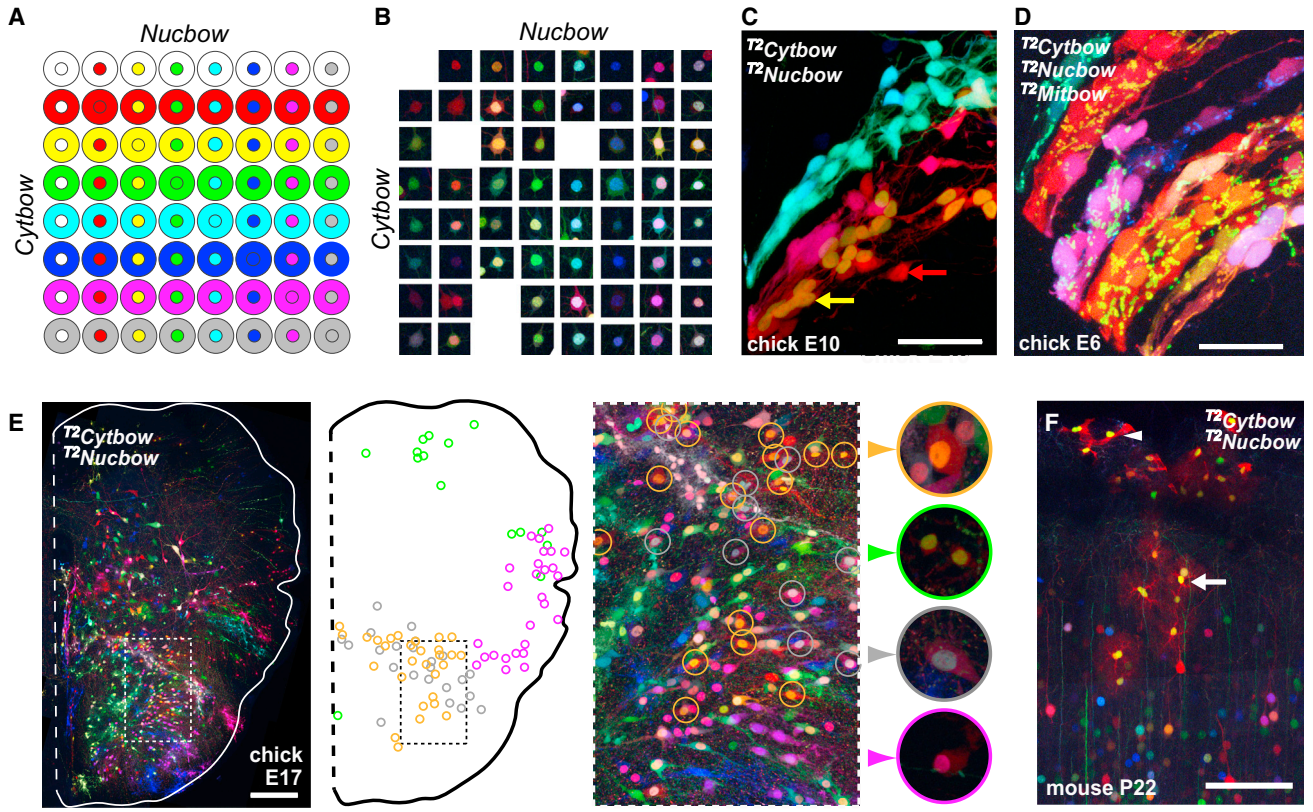

Figure 7. Clonal Identification with Dual-Targeted Brainbow Markers

(A) Multicopy Brainbow expression in two subcellular compartments provides a series of new labels to distinguish cells (also see Figure S7).

(B) Multiple distinct marker combinations are expressed in P28 mouse cortical neurons after coelectroporation with *T2Nucbow* and *T2Cytbow* at E13.

(C and D) Transverse sections of chick spinal cord electroporated at E2 with *T2Cytbow* and *T2Nucbow* (C) or *T2Cytbow*, *T2Nucbow*, and *T2Mitbow* (D). At E10 (C) and E6 (D), radially migrating clones can be identified based on the proportion and subcellular localization of FP color markers. In (C), two overlapping clones showing a similar "red" cytoplasmic staining can be distinguished on the basis of their expression of a different nuclear color (yellow and red arrows).

(E) In E17 spinal cords coexpressing *T2Cytbow* and *T2Nucbow*, an extensive palette of marker combinations is observed in differentiated glial and neuronal cells (see Figure S6). Specific combinations of markers identify potentially clonal groups of cells distributed in circumscribed areas.

(F) View of a P22 mouse cortex electroporated with *T2Cytbow* and *T2Nucbow* at E13. An astrocyte clone labeled with cytoplasmic red and yellow-green nuclei is found to include both protoplasmic (arrow) and fibrous (arrowhead) astrocytes.

Scale bars represent 45 μm (C and D), 100 μm (E), or 70 μm (F).

and S6, Movie S3). Some of these clones contained morphologically diverse cells (Figure S6). In the mouse cortex, the unique categories resulting from *T2Cytbow* and *T2Nucbow* cointegration at E13 also secured identification of astrocyte clones at P22. Remarkably, although some clones comprised only one morphological type of astrocytes—either protoplasmic or fibrous, as previously described (Garcia-Marques and Lopez-Mascaraque, 2013)—we observed that other clones included both (n = 12, 5 animals, Figure 7F).

Stability of MAGIC Markers during Multilineage Clonal Expansion

The stability of FP marker combinations during development is crucial for reliable clonal identification. We sought to further examine the potential impact of differential transgene silencing when tracking clonally related cells in long-term experiments and over different cell lineages. The retina provided an ideal model to address this question, with neurogenic progenitors giving rise to several cell types (photoreceptor, bipolar, horizontal, amacrine, and ganglion cells as well as Müller glia) that segregate in three well-distinct layers, the outer and inner nuclear layers (ONL and INL) and the ganglion cell layer (GCL). Retinal clones derived from single neurogenic progenitors typically maintain a tight columnar organization (Fekete et al., 1994) and can be resolved in sparsely labeled samples. We electroporated chick optic vesicles during the period of progenitor amplification (E1.5), before retinal progenitors switch to the neurogenic mode, and analyzed retina in whole-mount preparations at E15 (Figure 8). Large groups of cells were labeled with similar colors indicating a shared pattern of transgene integration. Each of these clonal groups could be further divided in several spatially segregated subgroups harboring the multiple cell types and typical columnar organization of retinal clones. This allowed us to investigate color stability during differentiation, both (1) *between* cell types by comparing cells with distinct identities *within* columnar subclones, and (2) *within* cell types by

comparing cells of a same identity *between* columns belonging to a same clonal group.

In the sample shown in Figures 8A and 8B, we analyzed six large color groups each composed of multiple (>6) columns. For each color group, we plotted the color content of 2–5 clonal columns (n = 120–430 cells per color group) and analyzed its dispersion as a function of radial position (Figure 8B). Within each column, relative FP proportions were in most cases homogeneous among cells of a same type (as evidenced by their morphology and radial position). Remarkably, this conservation extended to neighboring columns within the clonal group (Figure 8B, also see Figure 8A). Between cell types (i.e., between different retinal layers), FP proportions were also conserved, although more divergence was observed than within cell types. In a few cases, cells belonging to a same type displayed divergent colors (e.g., retinal ganglion cells and amacrine cells of clonal group *e*, Figure 8B). We hypothesize that this divergence could reflect the known subtype heterogeneity of these cells. Remarkably, it was also reproducible between columns of a same clonal group, suggesting that within a clonal population, MAGIC markers may reflect reproducible silencing effects in certain cell types or subtypes. Although in the example provided, color divergence appeared stronger in clones with complex FP combinations, it should be noted that, because insertion sites are random, the amount of interlineage variability cannot be predicted and may differ between samples.

Therefore, FP marker combinations appeared broadly stable within cells of a same type and in many cases between cell types, but as in all lineage-tracing methods based on expression of genomic reporters (Buckingham and Meilhac, 2011; Petit et al., 2005), their conservation could in some cases be affected by differential silencing during differentiation.

DISCUSSION

Multicolor Labeling with Regulated Sparseness

Genetic engineering provides an expanding range of options for high information content imaging in intact tissues by using FP spectral variants to resolve cells and encode their lineage relationships (Buckingham and Meilhac, 2011; Jefferis and Livet, 2012; Kretzschmar and Watt, 2012). Although recent studies used up to six different FPs (Garcia-Marques and Lopez-Mascaraque, 2013; Malide et al., 2012), we chose to rely on three FPs markers that can be optimally separated and offer full compatibility with recent multiphoton excitation methods (Figures 1E, 2, 3D, and 4B; Mahou et al., 2012). These FPs can generate multicolor patterns of varied complexity. Mostly mutually exclusive FPs are observed in transgenic mice reported in this study (Figure S1), indicating expression from few independent transgene copies as in other recent multicolor reporter lines (Ghigo et al., 2013; Rinkevich et al., 2011; Snippert et al., 2010). Embryonic electroporation provides a new way to generate FP combinations through coexpression of Brainbow transgenes, in numbers that depend on the experimental conditions: electroporation of nonintegrative *Cytbow* generates a large palette of unsaturated colors indicative of FP coexpression at near-equal levels from many episomal vector copies (Figures 1D and S2A), whereas genome-integrative vectors typically yield discrete, saturated colors, in accordance with expression from a limited number of transgenes. In ^{T2}*Cytbow*-labeled mouse forebrains, six to ten colors expressed by cortical astrocytes and olfactory interneurons suggest that one to three integrated transposons are active in these cells (Figures 4 and S4). In the embryonic chicken spinal cord and retina, complex FP mixtures demonstrate efficient multicopy integration (Figures 3A–3D, 6, and 8).

Importantly, the transgenes presented here offer the possibility to regulate labeling sparseness without affecting the balance between FP color markers, because they restrict expression of the three "RGB" markers exploited for clonal identification to cells that are subject to Cre recombination. Embryonic electroporation offers a convenient way to tune labeling frequency by changing plasmid ratios and electroporation conditions (e.g., Figures 3A–3D), and to target expression in specific, focal areas. Achieving sparse multicolor labeling facilitates identification and segmentation of individual neural cells compared to first and second generation *Brainbow-1.0* animals (Ghigo et al., 2013; Gupta and Poss, 2012; Livet et al., 2007; Tabansky et al., 2013) in which a red FP is expressed by default throughout the brain (Figures S1C, S1D, S2, S3E, and S3F).

Clonal Analysis with MAGIC Markers

Clonal tracking requires labeling of individual progenitors with markers that are stable over time and faithfully transmitted through cell division. This is ensured by the genome integration of multicolor reporter transgenes, achieved here either in transgenic animals, as done previously in rodent (Ghigo et al., 2013; Rinkevich et al., 2011; Snippert et al., 2010; Tabansky et al., 2013), fish (Pan et al., 2013), or insect models (Hadjieconomou et al., 2011; Hampel et al., 2011) or through the association of embryonic electroporation and transposon vector integration (Chen and LoTurco, 2012; Garcia-Marques and Lopez-Mascaraque, 2013; Sato et al., 2007; Yoshida et al., 2010). Combining this second approach with Brainbow provides an attractive alternative to transgenic animals, yielding rich combinations of FP markers expressed from multiple independent transgene copies. In proliferating progenitors electroporated with Brainbow transposons, expression from genome-integrated transgenes becomes rapidly dominant as cell divisions eliminate remaining episomes. We show that the resulting color labels (that is, the relative FP proportions expressed by labeled cells) cluster within embryonic neural clones and can be used in a quantitative manner for identifying clonally related cells (Figure 6). Measurements in different contexts presented in this study indicate that color content is generally stable during clonal expansion within homogeneous cell populations (Figures 6 and 8) but may in some cases vary as cells acquire different identities (Figure 8). This most likely reflects differential epigenetic regulation occurring at insertion loci as a result of cell differentiation—indeed, the *CAG* promoter used here, although broadly active, can be affected by positional effects. As such, using color labels resulting from coexpression of multiple transgene copies represents a trade-off: on one hand, increasing transgene copy number augments the palette of label combinations and their discriminatory power; on the other hand, it augments the probability that

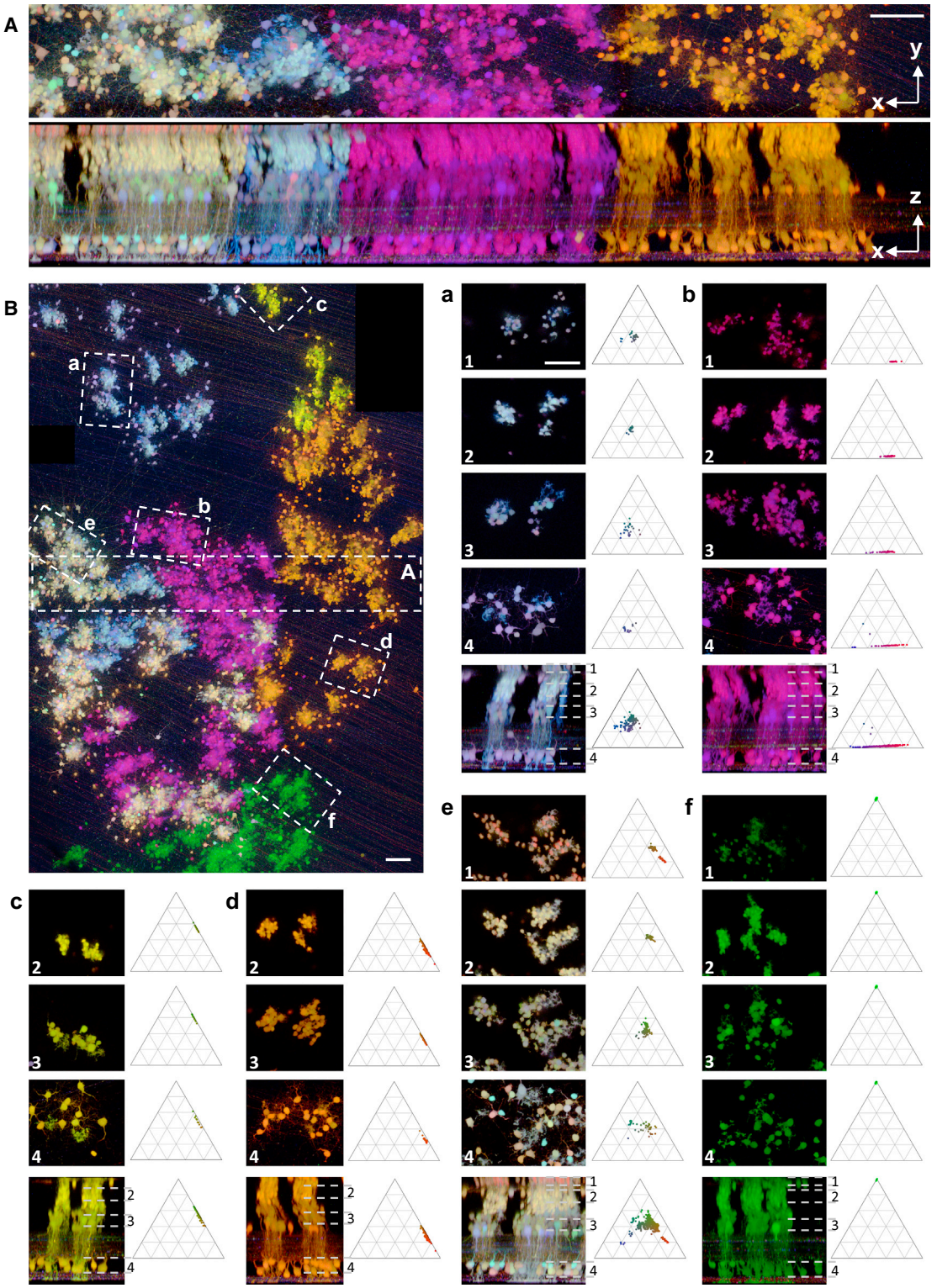

Figure 8. Color Stability in Multilineage Clones

Label conservation within complex clones comprising distinct cell types was investigated in the late-embryonic chick retina. Sparse labeling during progenitor amplification at E1.5 yielded large clonal groups composed of several spatially segregated subclones at E15.

(A) En-face view (top) and radial projection (bottom) of a ^{T2}*Cytbow*-labeled E15 retina. The radial view reveals the layered and columnar organization of labeled clonal groups.

(legend continued on next page)

one copy may be silenced by epigenetic effects. Interestingly, MAGIC markers can then provide a readout of these silencing effects (Figure 8). Although epigenetic silencing may be controlled by inserting Brainbow transgenes in an ubiquitous locus (Rinkevich et al., 2011; Snippert et al., 2010), so far only 3–4 distinct colors have been expressed in this manner.

Another aspect essential for clonal identification is to target progenitor cells with unique, distinct markers. Multicolor strategies provide a palette of markers that subdivide a global labeling pattern and can achieve uniqueness if expressed with sufficient sparseness. The success of the strategy relies on the adequacy between labeling density, clonal dispersion, and the number of color combinations that can be distinguished, and we foresee that the perfect match will differ from one experimental paradigm to another. MAGIC markers present several advantages along these lines. As seen above, labeling sparseness can be regulated by tuning recombination frequency and a large palette of clonal labels can be created by combinatorial FP expression from multiple genome-integrated vectors. Compartmentalized labeling further improves the discriminative power of color labels (Figure S7). For instance, simply considering qualitative differences in FP expression from 1–3 integrated copies of Brainbow transgenes targeting two cellular compartments offers up to 53 distinct labels, instead of 13 for a single subcellular compartment (Figure S7A). In situations with high copy number, the probability that two adjacent clones will harbor indistinguishable color combinations in two subcellular compartments is also greatly reduced compared to one single compartment (Figure S7B). Importantly, all the different marker combinations are not equiprobable (Figure 6G), such that even in the case of relatively dense labeling, rare labels can be used to single-out individual clones.

By allowing ubiquitous Cre-dependent expression of FP combinations addressed to multiple subcellular compartments, MAGIC markers generalize approaches recently introduced to label astrocytes with mixtures of transposon vectors encoding nuclear and cytoplasmic FPs from a glial-specific promoter (Garcia-Marques and Lopez-Mascaraque, 2013). With this methodology, neighboring clones can be compared and their spatial relationships revealed. This approach should prove useful for assaying progenitor equivalence and clonal interactions during nervous system development as previously done in simpler models (Ghigo et al., 2013; Gupta and Poss, 2012; Rinkevich et al., 2011; Snippert et al., 2010; Tabansky et al., 2013). We also show that color labels are applicable to track neural progenitors and their descent in long-term experiments, from embryonic to adult stages. Strikingly, for instance, labels delivered in dividing mouse cortical progenitors during embryonic neurogenesis were maintained in the postnatal neurogenic cells, giving rise to olfactory bulb interneurons (Figure 4).

Multiple Outcome Mosaic Analysis

Brainbow transgenes, despite being used thus far only for anatomical and lineage purposes, create a Cre-dependent genetic mosaic with multiple, stochastically determined states that are ideal for functional mosaic analysis. Our data show that MAGIC marker colors can provide a readout of the perturbation induced by a specific molecular determinant (Figure 5). This strategy is adaptable to a variety of interactors and offers a way to compare both perturbed and control situations within a given embryo, alleviating some of the variability linked to the electroporation method. It opens new possibilities to study the autonomous and nonautonomous roles of molecular determinants.

In conclusion, the MAGIC marker scheme is universally applicable to achieve stable multicolor expression with regulated sparseness in subsets of neural progenitors. The Cre dependence of the transgenes makes them compatible with the large number of Cre driver mice available to restrict labeling to specific cell types. Transposons can be used in a wide spectrum of animal models, in combination with electroporation or other transfection methods. With constant improvements in imaging of intact tissue (Chung et al., 2013; Ragan et al., 2012), we anticipate that multiclonal labeling with MAGIC markers should facilitate morphological, lineage, and functional analysis in a variety of experimental contexts.

EXPERIMENTAL PROCEDURES

Transgene Design

Brainbow transgenes were assembled according to a *Brainbow-1.1* blueprint (Livet et al., 2007) with the following FPs: EBFP2 (Ai et al., 2007), mCerulean (Rizzo et al., 2004), mTurquoise2 (Goedhart et al., 2012), mEYFP (Zacharias et al., 2002), and tdTomato or mCherry (Shaner et al., 2004). The *Nucbow*, *Palmbow*, and *Mitbow* transgenes were built with Histone-2B sequences, palmitoylation signals, or mitochondria-targeting sequences, respectively. Integrative vectors were produced by cloning the corresponding transgenes in a custom plasmid bearing *5′* and *3′ Tol2* or *Piggybac* transposition sequences (Lacoste et al., 2009; Yoshida et al., 2010). To build the ^{T2}*LGNbow* construct, the dominant-negative LGN followed by a 2A cleavage sequence was inserted in ^{T2}*Cytbow* upstream of *mCerulean* with BspEI and SacI. Further details are provided in Supplemental Experimental Procedures. Detailed maps and sequences of the vectors are available upon request.

Animals

Mice were housed in a 14 hr light/10 hr dark cycle with free access to food, and animal procedures were carried out in accordance with institutional guidelines. Transgenic mouse lines were generated by pronuclear injection of the *CAG-Nucbow* and *CAG-Cytbow* transgenes linearized with HindIII and MluI. A total of two to four independent lines showing Cre-dependent FP expression were established for each construct. Mice were crossed with *CAG-CreERTM*

(B) Low-magnification view of the same retina, showing the broad spatial dispersion of six clonal populations, each comprising multiple spatially arrayed subclones. The region shown in (A) and six smaller subclonal areas (a–f) are highlighted. For each subclonal area, maximal projections within three (c, d) or four (a, b, e, f) layers containing distinct cell types are displayed above a radial projection of the whole volume. Ternary plots show the mean RGB values of all cells contained in the projected volume. Within a clone, color content is generally homogeneous among cells of a same type (e.g., a2-3, b1-2, c2-4, d3-4), whereas color dispersion is more pronounced between different cell types (e.g., compare a2 and a4, e1 and e3), suggesting cell-type-specific differential regulation of $\geq$2 integrated transgenes.

Numbering: 1, ONL-containing photoreceptors; 2, external part of the INL containing bipolar cells and some Müller glia; 3, internal INL, with amacrine and Müller cells; 4, GCL, containing ganglion cells and displaced amacrine cells. Scale bars represent 50 μm.

animals and recombination was induced at E9.5 and P0 with tamoxifen as in Livet et al. (2007). In utero and in ovo electroporation were performed as described (Loulier et al., 2009; Morin et al., 2007; Sakuta et al., 2008). See Table S1 for the concentrations of DNA solutions and Supplemental Experimental Procedures for details.

Histology

Tissues were fixed in 4% paraformaldehyde. 20 μm sections of embryonic mouse brains were obtained with a cryostat. Adult mouse brain and E10–E17 chick spinal cords were sectioned at 200–400 μm thickness with a vibrating-blade microtome. Chick E7 spinal cords and E15 retina were flat-mounted on glass slides. Immunohistology was performed on free-floating sections with goat anti-Olig2 (R&D) and rabbit anti-S100β (gift of N. Ropert) antibodies. Samples were mounted in Vectashield mounting medium (Vector Labs).

Imaging

Epifluorescence images were collected with 5 × 0.4 NA and 10 × 0.6 NA objectives on a Leica DM6000 microscope equipped with a VT1000 camera. Confocal image stacks were acquired with 20 × 0.8 NA and 40 × 1.3 NA objectives on an Olympus FV1000 microscope, with 405, 440, 515, 560, and 633 nm laser lines to separately excite EBFP2, mCerulean/mTurquoise2, mEYFP, tdTomato/mCherry, and Alexa 647/Cy5, respectively. Two-photon imaging was performed on a custom-built point-scanning two-photon microscope with a 25 × 1.05 NA objective (Olympus) and the wavelength mixing method described in Mahou et al. (2012).

Image and Color Analysis

In all figures, tdTomato/mCherry, mEYFP, and mCerulean/mTurquoise2 are rendered in red, green, and blue, respectively. Image analysis was performed with Fiji (Schindelin et al., 2012), Matlab (MathWorks), and Imaris (Bitplane). A custom interface allowed us to segment regions of interest and extract pixel values from labeled cells. The segmentation interface, the plotting codes, a representative data set, and detailed instructions are available as a downloadable package. Ternary graphs show the relative weight of each color channel $C_{R,G,B} = (I_{R,G,B} - I_{minR,minG,minB})/(I_R + I_G + I_B)$, where $I_{R,G,B}$, I_R, I_G, I_B, and $I_{minR,\ minG,\ minB}$ are the intensities and minimal intensity values for each color channel, respectively.

SUPPLEMENTAL INFORMATION

Supplemental Information includes Supplemental Experimental Procedures, seven figures, one table, and three movies and can be found with this article online at http://dx.doi.org/10.1016/j.neuron.2013.12.016.

ACKNOWLEDGMENTS

We thank D. Débarre, T. Misgeld, L. Godinho, M. Saadaoui, S. Tozer, J.G. Corbin, J. Bradley, R.M. Gould, J.-L. Martin, and J.-A. Sahel for helpful comments and discussions and S. Sharma, K. Morita, and S. Clavreul for assistance with experiments and analysis. We acknowledge N. Ropert for the anti-S100β antibody, S. Ylä-Herttuala for the *se-Cre* plasmid, and M. Wassef for chicken equipment. We thank C. Martin and the SEAT team for pronuclear injections and the IdV animal facility for animal care. This work was supported by French State funds managed by the ANR within the Investissements d'Avenir programme under references ANR-10-LABX-65 (LabEx LifeSenses), ANR-10-INBS-04 (France-BioImaging), ANR-11-IDEX-0004-02, ANR-10-LABX-54 (LabEx MemoLife) and ANR-11-IDEX-0001-02 (PSL* Research University), ANR-2010-JCJC-1411, ANR-2010-JCJC-1510-01, Ville de Paris (recherche médicale et santé), Ecole des Neurosciences de Paris Ile-de-France (ENP), Inserm Avenir, and a Marie Curie International Reintegration Grant within the 7th European Community Framework Programme (PIRG06-GA-2009-256518).

Accepted: December 3, 2013
Published: February 5, 2014

REFERENCES

Ai, H.W., Shaner, N.C., Cheng, Z., Tsien, R.Y., and Campbell, R.E. (2007). Exploration of new chromophore structures leads to the identification of improved blue fluorescent proteins. Biochemistry *46*, 5904–5910.

Badea, T.C., Wang, Y., and Nathans, J. (2003). A noninvasive genetic/pharmacologic strategy for visualizing cell morphology and clonal relationships in the mouse. J. Neurosci. *23*, 2314–2322.

Birling, M.C., Gofflot, F., and Warot, X. (2009). Site-specific recombinases for manipulation of the mouse genome. Methods Mol. Biol. *561*, 245–263.

Buckingham, M.E., and Meilhac, S.M. (2011). Tracing cells for tracking cell lineage and clonal behavior. Dev. Cell *21*, 394–409.

Cai, D., Cohen, K.B., Luo, T., Lichtman, J.W., and Sanes, J.R. (2013). Improved tools for the Brainbow toolbox. Nat. Methods *10*, 540–547.

Carlson, C.A., Kas, A., Kirkwood, R., Hays, L.E., Preston, B.D., Salipante, S.J., and Horwitz, M.S. (2012). Decoding cell lineage from acquired mutations using arbitrary deep sequencing. Nat. Methods *9*, 78–80.

Chen, F., and LoTurco, J. (2012). A method for stable transgenesis of radial glia lineage in rat neocortex by piggyBac mediated transposition. J. Neurosci. Methods *207*, 172–180.

Chung, K., Wallace, J., Kim, S.Y., Kalyanasundaram, S., Andalman, A.S., Davidson, T.J., Mirzabekov, J.J., Zalocusky, K.A., Mattis, J., Denisin, A.K., et al. (2013). Structural and molecular interrogation of intact biological systems. Nature *497*, 332–337.

De Gasperi, R., Rocher, A.B., Sosa, M.A., Wearne, S.L., Perez, G.M., Friedrich, V.L., Jr., Hof, P.R., and Elder, G.A. (2008). The IRG mouse: a two-color fluorescent reporter for assessing Cre-mediated recombination and imaging complex cellular relationships in situ. Genesis *46*, 308–317.

Fekete, D.M., Perez-Miguelsanz, J., Ryder, E.F., and Cepko, C.L. (1994). Clonal analysis in the chicken retina reveals tangential dispersion of clonally related cells. Dev. Biol. *166*, 666–682.

Garcia-Marques, J., and Lopez-Mascaraque, L. (2013). Clonal identity determines astrocyte cortical heterogeneity. Cereb. Cortex *23*, 1463–1472.

Ge, W.P., Miyawaki, A., Gage, F.H., Jan, Y.N., and Jan, L.Y. (2012). Local generation of glia is a major astrocyte source in postnatal cortex. Nature *484*, 376–380.

Ghigo, C., Mondor, I., Jorquera, A., Nowak, J., Wienert, S., Zahner, S.P., Clausen, B.E., Luche, H., Malissen, B., Klauschen, F., and Bajénoff, M. (2013). Multicolor fate mapping of Langerhans cell homeostasis. J. Exp. Med. *210*, 1657–1664.

Goedhart, J., von Stetten, D., Noirclerc-Savoye, M., Lelimousin, M., Joosen, L., Hink, M.A., van Weeren, L., Gadella, T.W., Jr., and Royant, A. (2012). Structure-guided evolution of cyan fluorescent proteins towards a quantum yield of 93%. Nat. Commun. *3*, 751.

Gupta, V., and Poss, K.D. (2012). Clonally dominant cardiomyocytes direct heart morphogenesis. Nature *484*, 479–484.

Hadjieconomou, D., Rotkopf, S., Alexandre, C., Bell, D.M., Dickson, B.J., and Salecker, I. (2011). Flybow: genetic multicolor cell labeling for neural circuit analysis in *Drosophila melanogaster*. Nat. Methods *8*, 260–266.

Hampel, S., Chung, P., McKellar, C.E., Hall, D., Looger, L.L., and Simpson, J.H. (2011). *Drosophila* Brainbow: a recombinase-based fluorescence labeling technique to subdivide neural expression patterns. Nat. Methods *8*, 253–259.

Jefferis, G.S., and Livet, J. (2012). Sparse and combinatorial neuron labelling. Curr. Opin. Neurobiol. *22*, 101–110.

Kobiler, O., Lipman, Y., Therkelsen, K., Daubechies, I., and Enquist, L.W. (2010). Herpesviruses carrying a Brainbow cassette reveal replication and expression of limited numbers of incoming genomes. Nat. Commun. *1*, 146.

Kohwi, M., Petryniak, M.A., Long, J.E., Ekker, M., Obata, K., Yanagawa, Y., Rubenstein, J.L., and Alvarez-Buylla, A. (2007). A subpopulation of olfactory bulb GABAergic interneurons is derived from Emx1- and Dlx5/6-expressing progenitors. J. Neurosci. *27*, 6878–6891.

Konno, D., Shioi, G., Shitamukai, A., Mori, A., Kiyonari, H., Miyata, T., and Matsuzaki, F. (2008). Neuroepithelial progenitors undergo LGN-dependent planar divisions to maintain self-renewability during mammalian neurogenesis. Nat. Cell Biol. *10*, 93–101.

Kretzschmar, K., and Watt, F.M. (2012). Lineage tracing. Cell *148*, 33–45.

Kuan, C.Y., Elliott, E.A., Flavell, R.A., and Rakic, P. (1997). Restrictive clonal allocation in the chimeric mouse brain. Proc. Natl. Acad. Sci. USA *94*, 3374–3379.

Lacoste, A., Berenshteyn, F., and Brivanlou, A.H. (2009). An efficient and reversible transposable system for gene delivery and lineage-specific differentiation in human embryonic stem cells. Cell Stem Cell *5*, 332–342.

Leber, S.M., and Sanes, J.R. (1995). Migratory paths of neurons and glia in the embryonic chick spinal cord. J. Neurosci. *15*, 1236–1248.

Li, Y., Lu, H., Cheng, P.L., Ge, S., Xu, H., Shi, S.H., and Dan, Y. (2012). Clonally related visual cortical neurons show similar stimulus feature selectivity. Nature *486*, 118–121.

Livet, J., Weissman, T.A., Kang, H., Draft, R.W., Lu, J., Bennis, R.A., Sanes, J.R., and Lichtman, J.W. (2007). Transgenic strategies for combinatorial expression of fluorescent proteins in the nervous system. Nature *450*, 56–62.

Loulier, K., Lathia, J.D., Marthiens, V., Relucio, J., Mughal, M.R., Tang, S.C., Coksaygan, T., Hall, P.E., Chigurupati, S., Patton, B., et al. (2009). beta1 integrin maintains integrity of the embryonic neocortical stem cell niche. PLoS Biol. *7*, e1000176.

Magavi, S., Friedmann, D., Banks, G., Stolfi, A., and Lois, C. (2012). Coincident generation of pyramidal neurons and protoplasmic astrocytes in neocortical columns. J. Neurosci. *32*, 4762–4772.

Mähönen, A.J., Airenne, K.J., Lind, M.M., Lesch, H.P., and Ylä-Herttuala, S. (2004). Optimized self-excising Cre-expression cassette for mammalian cells. Biochem. Biophys. Res. Commun. *320*, 366–371.

Mahou, P., Zimmerley, M., Loulier, K., Matho, K.S., Labroille, G., Morin, X., Supatto, W., Livet, J., Débarre, D., and Beaurepaire, E. (2012). Multicolor two-photon tissue imaging by wavelength mixing. Nat. Methods *9*, 815–818.

Malide, D., Métais, J.Y., and Dunbar, C.E. (2012). Dynamic clonal analysis of murine hematopoietic stem and progenitor cells marked by 5 fluorescent proteins using confocal and multiphoton microscopy. Blood *120*, e105–e116.

Mathis, L., and Nicolas, J.F. (2003). Progressive restriction of cell fates in relation to neuroepithelial cell mingling in the mouse cerebellum. Dev. Biol. *258*, 20–31.

Matsuda, T., and Cepko, C.L. (2007). Controlled expression of transgenes introduced by in vivo electroporation. Proc. Natl. Acad. Sci. USA *104*, 1027–1032.

Morin, X., Jaouen, F., and Durbec, P. (2007). Control of planar divisions by the G-protein regulator LGN maintains progenitors in the chick neuroepithelium. Nat. Neurosci. *10*, 1440–1448.

Muzumdar, M.D., Tasic, B., Miyamichi, K., Li, L., and Luo, L. (2007). A global double-fluorescent Cre reporter mouse. Genesis *45*, 593–605.

Niwa, H., Yamamura, K., and Miyazaki, J. (1991). Efficient selection for high-expression transfectants with a novel eukaryotic vector. Gene *108*, 193–199.

Noctor, S.C., Flint, A.C., Weissman, T.A., Dammerman, R.S., and Kriegstein, A.R. (2001). Neurons derived from radial glial cells establish radial units in neocortex. Nature *409*, 714–720.

Ohtsuki, G., Nishiyama, M., Yoshida, T., Murakami, T., Histed, M., Lois, C., and Ohki, K. (2012). Similarity of visual selectivity among clonally related neurons in visual cortex. Neuron *75*, 65–72.

Pan, Y.A., Freundlich, T., Weissman, T.A., Schoppik, D., Wang, X.C., Zimmerman, S., Ciruna, B., Sanes, J.R., Lichtman, J.W., and Schier, A.F. (2013). Zebrabow: multispectral cell labeling for cell tracing and lineage analysis in zebrafish. Development *140*, 2835–2846.

Petit, A.C., Legué, E., and Nicolas, J.F. (2005). Methods in clonal analysis and applications. Reprod. Nutr. Dev. *45*, 321–339.

Price, J., Turner, D., and Cepko, C. (1987). Lineage analysis in the vertebrate nervous system by retrovirus-mediated gene transfer. Proc. Natl. Acad. Sci. USA *84*, 156–160.

Ragan, T., Kadiri, L.R., Venkataraju, K.U., Bahlmann, K., Sutin, J., Taranda, J., Arganda-Carreras, I., Kim, Y., Seung, H.S., and Osten, P. (2012). Serial two-photon tomography for automated ex vivo mouse brain imaging. Nat. Methods *9*, 255–258.

Rinkevich, Y., Lindau, P., Ueno, H., Longaker, M.T., and Weissman, I.L. (2011). Germ-layer and lineage-restricted stem/progenitors regenerate the mouse digit tip. Nature *476*, 409–413.

Rizzo, M.A., Springer, G.H., Granada, B., and Piston, D.W. (2004). An improved cyan fluorescent protein variant useful for FRET. Nat. Biotechnol. *22*, 445–449.

Sakuta, H., Suzuki, R., and Noda, M. (2008). Retrovirus vector-mediated gene transfer into the chick optic vesicle by in ovo electroporation. Dev. Growth Differ. *50*, 453–457.

Sato, Y., Kasai, T., Nakagawa, S., Tanabe, K., Watanabe, T., Kawakami, K., and Takahashi, Y. (2007). Stable integration and conditional expression of electroporated transgenes in chicken embryos. Dev. Biol. *305*, 616–624.

Schepers, A.G., Snippert, H.J., Stange, D.E., van den Born, M., van Es, J.H., van de Wetering, M., and Clevers, H. (2012). Lineage tracing reveals Lgr5+ stem cell activity in mouse intestinal adenomas. Science *337*, 730–735.

Schindelin, J., Arganda-Carreras, I., Frise, E., Kaynig, V., Longair, M., Pietzsch, T., Preibisch, S., Rueden, C., Saalfeld, S., Schmid, B., et al. (2012). Fiji: an open-source platform for biological-image analysis. Nat. Methods *9*, 676–682.

Shaner, N.C., Campbell, R.E., Steinbach, P.A., Giepmans, B.N., Palmer, A.E., and Tsien, R.Y. (2004). Improved monomeric red, orange and yellow fluorescent proteins derived from *Discosoma* sp. red fluorescent protein. Nat. Biotechnol. *22*, 1567–1572.

Shitamukai, A., Konno, D., and Matsuzaki, F. (2011). Oblique radial glial divisions in the developing mouse neocortex induce self-renewing progenitors outside the germinal zone that resemble primate outer subventricular zone progenitors. J. Neurosci. *31*, 3683–3695.

Snippert, H.J., van der Flier, L.G., Sato, T., van Es, J.H., van den Born, M., Kroon-Veenboer, C., Barker, N., Klein, A.M., van Rheenen, J., Simons, B.D., and Clevers, H. (2010). Intestinal crypt homeostasis results from neutral competition between symmetrically dividing Lgr5 stem cells. Cell *143*, 134–144.

Stancik, E.K., Navarro-Quiroga, I., Sellke, R., and Haydar, T.F. (2010). Heterogeneity in ventricular zone neural precursors contributes to neuronal fate diversity in the postnatal neocortex. J. Neurosci. *30*, 7028–7036.

Tabansky, I., Lenarcic, A., Draft, R.W., Loulier, K., Keskin, D.B., Rosains, J., Rivera-Feliciano, J., Lichtman, J.W., Livet, J., Stern, J.N., et al. (2013). Developmental bias in cleavage-stage mouse blastomeres. Curr. Biol. *23*, 21–31.

Tan, S.S., Faulkner-Jones, B., Breen, S.J., Walsh, M., Bertram, J.F., and Reese, B.E. (1995). Cell dispersion patterns in different cortical regions studied with an X-inactivated transgenic marker. Development *121*, 1029–1039.

Tasic, B., Miyamichi, K., Hippenmeyer, S., Dani, V.S., Zeng, H., Joo, W., Zong, H., Chen-Tsai, Y., and Luo, L. (2012). Extensions of MADM (mosaic analysis with double markers) in mice. PLoS ONE *7*, e33332.

Ueno, H., and Weissman, I.L. (2010). The origin and fate of yolk sac hematopoiesis: application of chimera analyses to developmental studies. Int. J. Dev. Biol. *54*, 1019–1031.

Walsh, C., and Cepko, C.L. (1992). Widespread dispersion of neuronal clones across functional regions of the cerebral cortex. Science *255*, 434–440.

Walsh, C., and Cepko, C.L. (1993). Clonal dispersion in proliferative layers of developing cerebral cortex. Nature *362*, 632–635.

Wasserstrom, A., Adar, R., Shefer, G., Frumkin, D., Itzkovitz, S., Stern, T., Shur, I., Zangi, L., Kaplan, S., Harmelin, A., et al. (2008). Reconstruction of cell lineage trees in mice. PLoS ONE *3*, e1939.

Weber, K., Thomaschewski, M., Warlich, M., Volz, T., Cornils, K., Niebuhr, B., Täger, M., Lütgehetmann, M., Pollok, J.M., Stocking, C., et al. (2011). RGB marking facilitates multicolor clonal cell tracking. Nat. Med. *17*, 504–509.

Yoshida, A., Yamaguchi, Y., Nonomura, K., Kawakami, K., Takahashi, Y., and Miura, M. (2010). Simultaneous expression of different transgenes in neurons and glia by combining in utero electroporation with the Tol2 transposon-mediated gene transfer system. Genes Cells *15*, 501–512.

Yu, Y.C., Bultje, R.S., Wang, X., and Shi, S.H. (2009). Specific synapses develop preferentially among sister excitatory neurons in the neocortex. Nature *458*, 501–504.

Yu, Y.C., He, S., Chen, S., Fu, Y., Brown, K.N., Yao, X.H., Ma, J., Gao, K.P., Sosinsky, G.E., Huang, K., and Shi, S.H. (2012). Preferential electrical coupling regulates neocortical lineage-dependent microcircuit assembly. Nature *486*, 113–117.

Zacharias, D.A., Violin, J.D., Newton, A.C., and Tsien, R.Y. (2002). Partitioning of lipid-modified monomeric GFPs into membrane microdomains of live cells. Science *296*, 913–916.

Zong, H., Espinosa, J.S., Su, H.H., Muzumdar, M.D., and Luo, L. (2005). Mosaic analysis with double markers in mice. Cell *121*, 479–492.